

Aligning Correlation Information for Domain Adaptation in Action Recognition

Yuecong Xu^a, Jianfei Yang^{a,*}, Haozhi Cao^a, Kezhi Mao^a, Jianxiong Yin^b,
Simon See^b

^a*School of Electrical and Electronic Engineering, Nanyang Technological University, 50 Nanyang Avenue, 639798, Singapore*

^b*NVIDIA AI Tech Center, 3 International Business Park Rd, #01-20A Nordic European center, 609927, Singapore*

Abstract

Domain adaptation (DA) approaches address domain shift and enable networks to be applied to different scenarios. Although various image DA approaches have been proposed in recent years, there is limited research towards video DA. This is partly due to the complexity in adapting the different modalities of features in videos, which includes the correlation features extracted as long-term dependencies of pixels across spatiotemporal dimensions. The correlation features are highly associated with action classes and proven their effectiveness in accurate video feature extraction through the supervised action recognition task. Yet correlation features of the same action would differ across domains due to domain shift. Therefore we propose a novel Adversarial Correlation Adaptation Network (ACAN) to align action videos by aligning pixel correlations. ACAN aims to minimize the distribution of correlation information, termed as *Pixel Correlation Discrepancy* (PCD). Additionally, video DA research is also limited by the lack of cross-domain video datasets with larger domain shifts. We, therefore, introduce a novel *HMDB-ARID* dataset with a larger domain shift caused by a larger statistical difference between domains. This dataset is built in an effort to leverage current datasets for dark video classification.

*Corresponding author

Email addresses: xuyu0014@e.ntu.edu.sg (Yuecong Xu), yang0478@e.ntu.edu.sg (Jianfei Yang), haozhi001@e.ntu.edu.sg (Haozhi Cao), ekzmao1@ntu.edu.sg (Kezhi Mao), jianxiong@nvidia.com (Jianxiong Yin), ssee@nvidia.com (Simon See)

Empirical results demonstrate the state-of-the-art performance of our proposed ACAN for both existing and the new video DA datasets.

Keywords: Domain Adaptation, Correlation, Adversarial, Action Recognition, Dark Videos.

1. Introduction

Action recognition has long been studied thanks to its applications in various fields. Despite achieving promising results, most research assumes that the distribution of the test data is in line with that of the train data. Meanwhile, due to the high cost of annotating videos, it is desirable if networks trained in one domain could be directly applied to another. However, significant decrease in performances are observed when networks are applied to cross-domain scenarios. To alleviate the impact of domain shift, studies have been conducted on unsupervised domain adaptation (UDA), which aims to leverage data from the labeled source domain to boost performance on the unlabeled target domain. Previously, UDA has been explored on image-based tasks, such as image recognition [1, 2, 3], object detection [4, 5, 6] and person re-identification [7].

Comparatively, there is limited research towards applying DA methods to videos for tasks such as action recognition. This is mainly due to the fact that videos contain data with more modalities, which complicates the adaptation process. Earlier works use the same adaptation strategies as that for image DA while utilizing 3D Convolutional Neural Networks (3D-CNNs) instead of 2D Convolutional Neural Networks (2D-CNNs) for feature extraction. Current improvements in DA methods for video tasks focus on improving alignment along the temporal direction. Such improvements are in line with the additional temporal information provided in videos compare to images. They are achieved mainly through applying attention mechanisms to features of video segments sampled across the temporal direction [8, 9]. Alternatively, auxiliary tasks such as clip order prediction [10] are utilized to extract robust temporal representation [11].

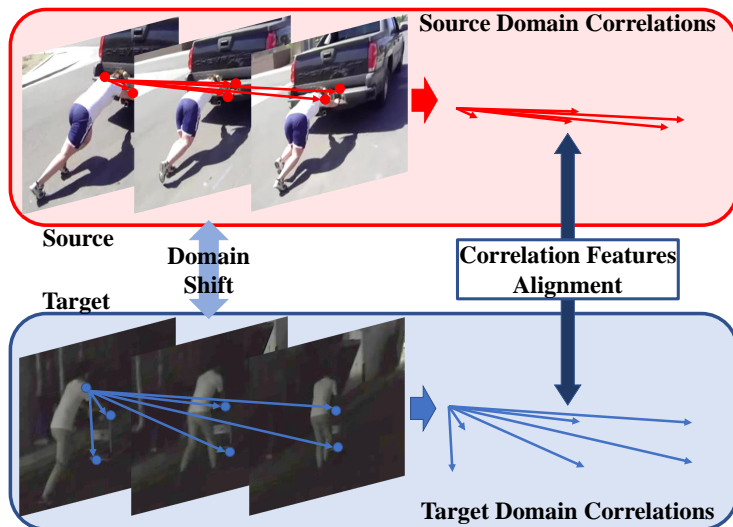


Figure 1: Illustration of our proposed correlation features alignment. The correlation features are extracted as long-term dependencies of pixels across spatiotemporal dimensions. For the same action in the source and target domains, their corresponding correlation features are distinct due to the different postures of the actors. While correlation features are highly associated with the action, alignment of video features should include the alignment of correlation features. Here we show two samples with the action “Push” from HMDB51 (top) and ARID (bottom).

Intuitively, the correlations between pixels are highly associated with an action. In supervised action recognition, such correlations have been recently exploited to aid the extraction of accurate video features. One significant example is the non-local neural network [12], inspired by the non-local mean operation for image denoising [13, 14]. The correlation features are extracted as long-term dependencies of pixels across spatiotemporal dimensions and construct spatiotemporal features by self-attention [15, 16, 17]. The correlation features have brought significant increase in network performance [12, 18, 19, 20, 21]. However, correlation features of the same action could be very different, as depicted in Figure 1. The same action “Push” sampled from two different datasets results in distinct correlations information. Given the close relation between

correlation features and the action, it is therefore reasonable to not only align spatial and temporal features alone but also to align correlation features. We therefore propose an Adversarial Correlation Adaptation Network (ACAN) that aligns correlation features in an adversarial manner.

For an action within a domain, its correlation features, and the embedded correlation information, would be similar, thanks to the similar appearance and postures of the actors. Yet outliers may be presented in each domain, which may impact the transferability of the network. To cope with this impact, we propose that the joint distribution of correlation information should be aligned. We believe that such a joint distribution of correlation information could be computed as the covariance of the correlation information [22], implemented as its corresponding Gram matrix [23]. Therefore, aligning the correlation features of two domains is interpreted as minimizing the difference between the Gram matrices of the correlation information. While direct minimization of the Gram matrix difference could come at a price of decreasing network discriminability and high computation cost, we propose to minimize the *pixel correlation discrepancy* (PCD).

Besides the complexity of the process of video data, the lack of research in DA methods for action recognition and other video-based tasks are also partly due to the lack of sufficient and meaningful cross-domain datasets. Apart from current video DA datasets, we proposed a new *HMDB-ARID* dataset from HMDB51 [24] and a recent dark video dataset, ARID [25]. The different illumination conditions of videos in HMDB51 and ARID causes larger domain shift, making the *HMDB-ARID* dataset more challenging.

Our main contributions are summarized as follows:

- * We proposed a novel ACAN network for domain adaptation in action recognition by aligning correlation features across domains.
- * We further improve the effectiveness of correlation alignment by aligning the joint distribution of correlation information of different domains through minimizing *pixel correlation discrepancy* (PCD).

- * We introduce a more challenging video DA dataset: the *HMDB-ARID* dataset. To our knowledge, this is the first video DA dataset that includes videos shot under different illumination.
- * We perform extensive experiments, whose results demonstrate the effectiveness of our proposed method, achieving state-of-the-art performance across multiple current and novel video DA datasets.

The rest of this paper is organized as follows: related works of unsupervised domain-adaptation in video-based tasks, such as action recognition are discussed in Section 2. In Section 3, we introduce our proposed Adversarial Correlation Adaptation Network (ACAN) with the process of minimizing *pixel correlation discrepancy* (PCD) thoroughly. Further, in Section 4, we introduce our proposed *HMDB-ARID* dataset in detail. After that, we present and analyze the experimental results of our proposed ACAN on previous and our novel video DA datasets, with a thorough ablation study on the design of ACAN in Section 5. Finally, we conclude the paper and propose our future work in Section 6.

2. Related Works

2.1. Action Recognition.

Action recognition has shown great progress with the use of CNNs for extracting accurate video features and representations. There exist mainly two branches of work. One of which utilizes the two-stream structure [26, 27, 28, 29, 30, 31, 32], extracting video features through CNNs from both optical flow and RGB inputs. The other path utilizes the 3D-CNN structure [33, 34, 35, 36, 37, 38, 39] to extract video features by extracting spatial and temporal features jointly with only RGB inputs. This path has made further progress by introducing separable CNN [40, 41], improving the efficiency of video feature extraction.

More recently, correlation information between pixels or features has been exploited for further improvements in action recognition. One significant example of which is inspired by the non-local means for image filtering task [13],

termed the non-local block [12], and is introduced with the non-local neural network for capturing correlation between pixels. Works as in [42, 18, 43] also improves video feature extraction using the same idea, but utilizing different methods such as attention [42, 18] or relation modules [43]. Despite the great progress made in action recognition, most models rely on the target supervised data for fine-tuning on the target dataset, and thus could not be applied to different domains or scenarios without sufficient labels or annotations. To this end, unsupervised domain adaptation helps improve the transferability of models so that they could be applied without access to target labels during training.

2.2. Unsupervised Domain Adaptation.

In recent years, there has been a rise of research interest in domain adaptation, which aims to distill shared knowledge across domains and improve the transferability of models. In our work, we focus on unsupervised domain adaptation (UDA), when labeled target data is not available. With the success of Generative Adversarial Network (GAN) [44], researchers have proposed to construct adversarial loss [1] for domain adaptation. Various adversarial based domain adaptation methods [1, 45, 46, 47, 3] have been proposed for a wide range of image-based tasks, such as image recognition [1, 2, 48, 3], object detection [4, 5, 49], semantic segmentation [50, 51, 52, 53] and person re-identification [54, 7].

Despite the progress in UDA for image-based tasks, there have been few works on UDA for video-based tasks (VUDA), such as action recognition [55, 8, 11, 9] and action segmentation [56]. Most of these works for action recognition adapt temporal features more effectively. However, none of them have explored the alignment of correlation features, which are highly associated with actions and proven its effectiveness in supervised tasks, yet may be very different across different domains. We therefore propose to align correlation information for better video feature alignment.

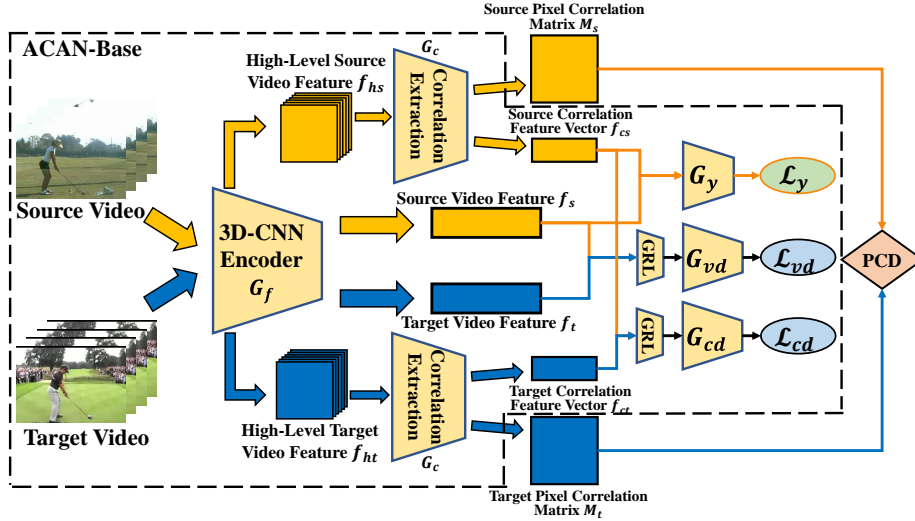


Figure 2: Overview of the structure of ACAN. We first generate video features with a shared 3D-CNN encoder for both source and target domain videos. The source and target correlation feature vectors are obtained through high-level video features, extracted from a deeper layer of the encoder. An adversarial domain loss is applied to both the video features and the correlation feature vectors for aligning the video features and correlation feature vectors. Further, aligning the joint correlation information distribution requires the alignment of the Gram matrices constructed from the pixel correlation matrices (PCM). To achieve this, we further introduce the pixel correlation discrepancy. Figure best viewed in color and zoomed in.

3. Method

In video UDA, we are given a source domain with N_s labeled videos $\mathcal{D}_s = \{(V_s^i, y_s^i)\}_{i=1}^{N_s}$, and a target domain with N_t unlabeled videos $\mathcal{D}_t = \{V_t^j\}_{j=1}^{N_t}$. The source and target domains are characterized by two underlying probability distributions p_s and p_t respectively. The goal of video UDA is to construct a network capable of learning transferable features and minimizing a target classification risk.

Current video DA approaches still rely on aligning only spatial and/or temporal features and fail to align correlation features which correlate long-term pixel dependencies. To cope with this challenge, we propose an Adversarial Cor-

relation Alignment Network (ACAN) to align cross-domain correlation features in an adversarial manner. We further introduce the *pixel correlation discrepancy* (PCD), motivated by the theoretical results in style transfer. We begin by presenting the base architecture of ACAN, followed by an illustration on the minimization of PCD.

3.1. Base Architecture

Figure 2 presents the base architecture of our proposed ACAN, illustrated as ACAN-Base. During training, given a source and target video pair (V_s^i, V_t^j) , the source and target video features f_s^i, f_t^j are obtained through a shared 3D-CNN encoder $G_f(\cdot; \theta_f)$. Meanwhile, the high-level source and target video feature f_{hs}^i, f_{ht}^j are extracted from a deeper layer of the 3D-CNN encoder (e.g. conv4 layer). The high-level video features are processed by a shared correlation extraction module G_c where the correlation features of the input videos are extracted. The results are the source and target correlation matrices $\mathbf{M}_s^i, \mathbf{M}_t^j$ as well as the source and target correlation feature vectors f_{cs}^i, f_{ct}^j . $G_c(\cdot; \theta_c)$ are built based on the non-local operation [12], which extracts the correlation features as long-range dependencies between spatiotemporal pixels. The source correlation feature vector and video feature f_{cs}^i, f_s^i are concatenated to form the overall feature representation of source video V_s^i , which would be input to a classifier G_y for action predictions. The action class prediction loss \mathcal{L}_y is computed with respect to the predictions from G_y , formulated as:

$$\mathcal{L}_y = \frac{1}{N_s} \sum_{i=1}^{N_s} L_y(G_y(f_{cs}^i \oplus f_s^i), y_i), \quad (1)$$

where L_y is the cross entropy loss function, and \oplus denotes the concatenation operation.

To accommodate the domain shift between source and target domains, adversarial-based UDA approaches are proved to perform well on image data [1, 45, 46, 47] and language data [57]. Therefore we also leverage this technique for VUDA, which aims to align the global distributions with additional domain discriminators that are trained with the feature generators in a min-max fashion.

Domain discriminators are designed to discriminate the video features while the feature generators are trained to deceive the domain discriminators. Here the feature generators are referred to as a combination of G_f and G_c . We adopted separate domain discriminators for the source/target video features f_*^* ($* \in (s, t), \star \in (i, j)$) and the source/target correlation features f_{c*}^* . The two domain discriminators are denoted as the video domain discriminator $G_{vd}(\cdot; \theta_{vd})$ and the correlation domain discriminator $G_{cd}(\cdot; \theta_{cd})$. During the adversarial training process, the parameters θ_{vd} and θ_{cd} are learned by minimizing the video domain loss \mathcal{L}_{vd} and the correlation domain loss \mathcal{L}_{cd} , respectively, which are formulated as:

$$\mathcal{L}_{vd} = \frac{1}{N_s} \sum_{i=1}^{N_s} L_b(G_{vd}(f_s^i), d_i) + \frac{1}{N_t} \sum_{j=1}^{N_t} L_b(G_{vd}(f_t^j), d_j), \quad (2)$$

$$\mathcal{L}_{cd} = \frac{1}{N_s} \sum_{i=1}^{N_s} L_b(G_{cd}(f_{cs}^i), d_i) + \frac{1}{N_t} \sum_{j=1}^{N_t} L_b(G_{cd}(f_{ct}^j), d_j), \quad (3)$$

where L_b is the binary cross-entropy loss of the domain discriminators, while d_i and d_j are the domain label for the source and target domains respectively. Meanwhile, the parameters of the feature extractors θ_f and θ_c are learned to maximize the domain losses. To achieve this, a Gradient Reverse Layer (GRL) is inserted before each domain discriminator as in Figure 2.

The overall loss function to be optimized can therefore be formulated as:

$$\mathcal{L} = \mathcal{L}_y - (\lambda_v \mathcal{L}_{vd} + \lambda_r \mathcal{L}_{cd}), \quad (4)$$

where λ_v and λ_r are the trade-off weights for the video domain loss and correlation domain loss respectively.

3.2. Minimizing Pixel Correlation Discrepancy

In the base ACAN network, the same DA approach is applied to both video and correlation features. However, it remains a question *whether such an approach is the most effective way for aligning correlation features across different domains?* Aligning correlation features can be further achieved through aligning the joint distribution of correlation information. The joint distribution could

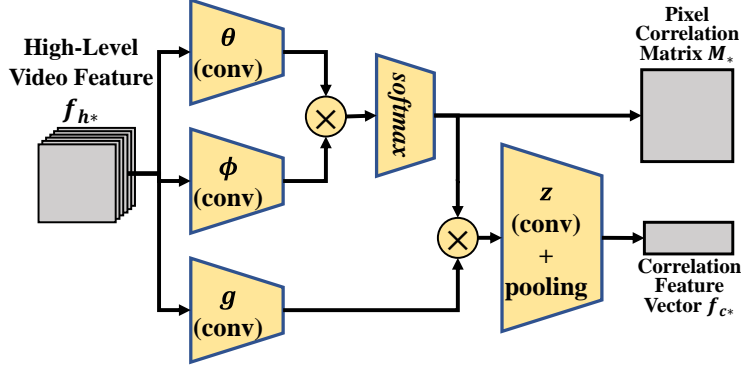


Figure 3: Structure of the correlation extraction module G_c . G_c extract correlation features (pixel correlation matrix \mathbf{M}_* and correlation feature vector f_{c*}) through the high-level video feature f_{h*} . It is built upon the non-local operation. \mathbf{M}_* is obtained through multiplication of f_{h*} projected on latent spaces, and represents the correlation between each spatio-temporal pixel feature. f_{c*} is further obtained by multiplying the $\mathbf{M}_* f_{h*}$ projected on the latent space, followed by pooling operation over spatiotemporal dimensions. The projection functions are implemented with convolution layers of $1 \times 1 \times 1$ kernel.

be computed as the covariance of correlation information, implemented as its corresponding Gram matrix. The key to the above question therefore lies in the expression of the correlation information. As illustrated in Figure 2, correlation features are extracted from G_c , whose structure is shown in Figure 3. For the i^{th} input video, we define the pixel correlation matrix (PCM) \mathbf{M}_*^i as:

$$\mathbf{M}_*^i = \varphi(\theta(f_{h*}^i)^T \phi(f_{h*}^i)), \quad (5)$$

where φ is the softmax operation. Both $\theta(\cdot)$ and $\phi(\cdot)$ are linear functions projecting the high-level video features to latent spaces. In practice, they are implemented as convolution layers with a kernel size of $1 \times 1 \times 1$. The value $\mathbf{M}_{*,pq}^i$ at the (p, q) position of PCM represents the correlation between the video feature at spatiotemporal point p, $f_{h*,p}^i$, and the video feature at spatiotemporal point q, $f_{h*,q}^i$. We argue that PCM could be viewed as the correlation information of the video. Therefore the joint correlation information distribution is constructed as the Gram matrix of the PCM, denoted as $\mathcal{G}^i \in \mathbb{R}^{N_M \times N_M}$, where

N_M is the number of spatiotemporal points in the feature map $\theta(f_{h^*}^i)$. \mathcal{G}^i is computed by:

$$\mathcal{G}^i = \mathbf{M}_*^{iT} \mathbf{M}_*^i. \quad (6)$$

The alignment of correlation features thus requires the minimization of the distance between the Gram matrices \mathcal{G} , termed as the video covariance loss \mathcal{L}_{vs} , formulated by:

$$\mathcal{L}_{vs} = \| \mathbf{E}(\mathcal{G}_s) - \mathbf{E}(\mathcal{G}_t) \|^2, \quad (7)$$

where the subscripts s and t denotes the Gram matrices for source and target videos respectively. However, such computation is inefficient, requiring a cost of $O(N_M^2)$. Furthermore, improving network transferability through minimizing \mathcal{L}_{vs} comes at the price of decreasing network discriminability. To minimize \mathcal{L}_{vs} more efficiently while causing less impact on the network’s discriminability, we simplify according to the theory in [58].

Theorem 1. *Given the Gram matrices $\mathcal{G}_s, \mathcal{G}_t$ constructed from source and target features $\mathbf{M}_s, \mathbf{M}_t$, the minimization of distance between the Gram matrices \mathcal{L}_{vs} can be seen as a distribution alignment process from \mathbf{M}_t to \mathbf{M}_s .*

As proven in [58], the theorem indicates that minimizing \mathcal{L}_{vs} could be reformulated as minimizing the distribution discrepancy of \mathbf{M}_t and \mathbf{M}_s . Set the underlying distributions of \mathbf{M}_s be p_{M_s} and that of \mathbf{M}_t be p_{M_t} . Here we propose the *pixel correlation discrepancy* (PCD), denote as $d_M(p_{M_s}, p_{M_t})$. Computing and minimizing this discrepancy is achieved by representing the distributions p_{M_s} and p_{M_t} as elements on the reproducing kernel Hilbert space (RKHS). As such, the distribution discrepancy could be defined as distance of distribution embedded elements on the RKHS.

Further, to align the distributions of p_{M_s} and p_{M_t} in a more fine-grained manner, it is important to align the distributions taking the relations between relevant classes into consideration. That is to align p_{M_s} and p_{M_t} within the same action classes in source and target domains, instead of aligning it only in

by the global distributions. The overall PCD is therefore formulated as:

$$d_M(p_{M_s}, p_{M_t}) \triangleq \mathbf{E}_c \|\mathbf{E}_{p_{M_s(c)}}[\zeta(\mathbf{M}_s)] - \mathbf{E}_{p_{M_t(c)}}[\zeta(\mathbf{M}_t)]\|_{\mathcal{H}}^2, \quad (8)$$

where $\mathbf{E}_{p_{M^*(c)}}$ is the mean embedding of distribution p_{M^*} for action class c on the RKHS \mathcal{H} . The feature map ζ is closely related to the RKHS characteristic kernel k by $k(\mathbf{M}_s, \mathbf{M}_t) = \langle \zeta(\mathbf{M}_s), \zeta(\mathbf{M}_t) \rangle$. The use of mean embedding for each class enables our PCD to align distributions of correlation information within each action class instead of only focusing on the global correlation information distribution. In practice, we may further assume that each video belongs to a certain action class with a class-related weight w_c . We therefore could estimate PCD in Equation 8 as:

$$d_M(p_{M_s}, p_{M_t}) = \frac{1}{C} \sum_{c=1}^C \left\| \sum_{i=1}^{N_s} w_{sc}^i \zeta(\mathbf{M}_s^i) - \sum_{j=1}^{N_t} w_{tc}^j \zeta(\mathbf{M}_t^j) \right\|_{\mathcal{H}}^2, \quad (9)$$

where C is the number of action classes. When computing the weight of a source video for a certain action class, given that the labels are provided, the weight w_{sc}^i is computed by:

$$w_{sc}^i = \frac{y_s^i}{\sum_{k=1}^{N_s} y_s^k}. \quad (10)$$

Whereas for the target videos, since the labels are not available, we cannot compute the weight w_{tc}^j directly. Instead, we utilize the output from the action classifier G_y which characterizes the probability of assigning a given video to an action class. This is denoted as the pseudo-label for a target video and is computed by:

$$y_t^j = G_y(f_{ct}^i \oplus f_t^i). \quad (11)$$

The resulting pseudo-labels of the target videos could be used as in Equation 10 for computing the weight of a target video for an action class. Finally, since the feature map ζ cannot be computed directly in most cases, we expand Equation 9 while utilizing the characteristic kernel k . The PCD could therefore be

Dataset	RGB Mean	RGB Std
HMDB51	[0.424,0.364,0.319]	[0.268,0.255,0.260]
UCF101	[0.409,0.397,0.358]	[0.266,0.265,0.270]
Kinetics	[0.432,0.395,0.377]	[0.228,0.222,0.217]
ARID	[0.079,0.074,0.073]	[0.101,0.098,0.090]

Table 1: Comparison of RGB mean and standard deviation (std) over common action recognition datasets and the ARID dataset.

reformulated as:

$$\begin{aligned}
d_M(p_{M_s}, p_{M_t}) = & \frac{1}{C} \sum_{c=1}^C \left(\sum_{i=1}^{N_s} \sum_{i'=1}^{N_s} w_{sc}^i w_{sc}^{i'} k(\mathbf{M}_s^i, \mathbf{M}_s^{i'}) \right. \\
& + \sum_{j=1}^{N_t} \sum_{j'=1}^{N_t} w_{tc}^j w_{tc}^{j'} k(\mathbf{M}_t^j, \mathbf{M}_t^{j'}) \\
& \left. - 2 \sum_{i=1}^{N_s} \sum_{j=1}^{N_t} w_{sc}^i w_{tc}^j k(\mathbf{M}_s^i, \mathbf{M}_t^j) \right), \tag{12}
\end{aligned}$$

where the kernel k would typically be of Gaussian form, hence $k(\mathbf{M}_s^i, \mathbf{M}_t^j) = -\exp(-\frac{\|\mathbf{M}_s^i - \mathbf{M}_t^j\|^2}{2\sigma^2})$. The overall optimization objective is thus formulated as:

$$\mathcal{L} = \mathcal{L}_y - (\lambda_v \mathcal{L}_{vd} + \lambda_r \mathcal{L}_{cd}) + \lambda_d d_M, \tag{13}$$

where λ_d is the trade-off weight for the PCD. Minimizing our proposed PCD is superior in effective alignment of cross-domain correlation features thanks to its relatively solid theoretical motivation. We find that aligning correlation features with other approaches without the proposed PCD (e.g. MMD [59], CORAL [60]) all produce inferior performances than our proposed approach, and would be illustrated in 5.

4. The HMDB-ARID Dataset

There are very limited cross-domain benchmark datasets for video DA tasks, therefore hindering the research for video DA. Previous cross-domain datasets introduced for video DA [61, 62, 55] are of very small-scale, with not more than

Statistics	<i>UCF-HMDB_{small}</i>	<i>UCF-Olympic</i>	<i>UCF-HMDB_{full}</i>	<i>HMDB-ARID</i>
Video Length (seconds)	1-21	1-39	1-33	1-30
Video Classes #	5	6	12	11
Training Video #	UCF:482/HMDB:350	UCF:601/Olympic:250	UCF:1438/HMDB:840	HMDB:770/ARID:2288
Validation Video #	UCF:189/HMDB:150	UCF:240/Olympic:54	UCF:571/HMDB:360	HMDB:330/ARID:823

Table 2: Comparison of current and our novel video DA datasets.

6 classes, and typically less than 1,000 videos. The lack of classes and data over these cross-domain datasets introduces limited domain discrepancy, and therefore the performances of DA approaches are saturated. More recently, larger cross-domain video datasets, such as *UCF-HMDB_{full}* have been introduced with larger domain discrepancies.

Though larger cross-domain datasets are introduced, both domains included in these datasets are still based on current well-established action recognition datasets. These action recognition datasets may include different classes with different videos, yet most of them are collected on public video platforms. This would lead to similar video statistics among these datasets, as compared in Table 1. Similar video statistics suggest high probability of similar scenarios exist among current action recognition datasets, thus the domain shift between these datasets may not be significant. Consequently, the difficulty of adapting the same model across the different domains with similar video statistics or similar scenarios may be trivial. Video DA approaches that perform well in these cross-domain video datasets may not be well applicable in real-world applications where the gap between domains may be much larger than current cross-domain datasets. We argue that video DA approaches would be more useful for bridging with video domains with large distribution shifts, such as dark videos (adverse illumination) or hazy videos (adverse contrast).

To explore how to leverage current datasets to boost performance on videos shot in adverse environments, we propose a novel cross-domain dataset. It incorporates both the current action recognition dataset and a more recent dark dataset, ARID [25], whose videos are shot under adverse illumination condi-

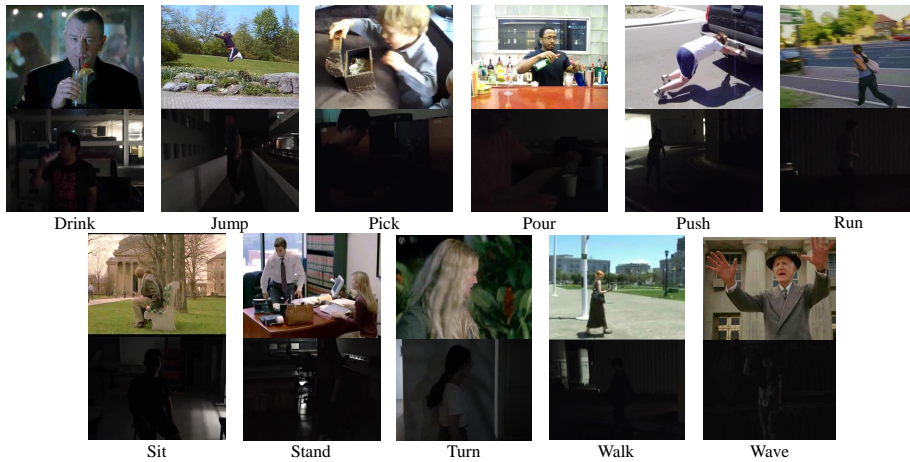


Figure 4: Sampled frames for each action class from the videos in *HMDB-ARID*. Note that the sampled frames from HMDB51 are shown in the upper row, whereas the sampled frame from ARID are shown in the lower row. Best viewed zoomed in.

tions. Compared with current action recognition datasets, videos in ARID are characterized by low brightness and low contrast. Statistically, videos in ARID possess much lower RGB mean value and standard deviation (std), as presented in Table 1. The larger statistical differences between ARID and current action recognition datasets, such as HMDB51 [24], would strongly suggest a larger domain shift between the different datasets.

The ARID dataset includes a total of 11 human action classes. These includes *drink*, *jump*, *pick*, *pour*, *push*, *run*, *sit*, *stand*, *turn*, *walk* and *wave*. When proposing the cross-domain *HMDB-ARID* dataset, we include all 11 action classes in ARID and HMDB51. For both datasets, we follow the official split method to separate the train and validation sets. The *HMDB-ARID* dataset thus includes 770 training videos and 330 validation videos from HMDB51, and 2288 training videos and 823 validation videos from ARID. Figure 4 shows the comparison of sampled frames from *HMDB-ARID* dataset. Compared to previous video DA datasets, besides containing larger domain shift, our dataset also contains a larger number of total videos for both training and validation,

as illustrated in Table 2.

5. Experiments

In this section, we evaluate our proposed ACAN performing cross-domain action recognition on two video DA datasets: *UCF-HMDB_{full}* and our new *HMDB-ARID*. We present state-of-the-art results on both datasets. We also present detailed ablation studies and qualitative analysis of our proposed ACAN to verify our design.

5.1. Experimental Settings and Details

We perform action recognition tasks on both the *UCF-HMDB_{full}* dataset and our new *HMDB-ARID* dataset. The *UCF-HMDB_{full}* dataset [8] is introduced as an expansion of the original *UCF-HMDB_{small}* dataset [61], with more classes and larger domain discrepancy. The *UCF-HMDB_{full}* contains a total of 3,209 videos with 12 action classes, all from the original UCF101 [63] and HMDB51 [24] datasets. It includes two settings: UCF→HMDB and HMDB→UCF, where the direction of the arrow symbol is set from the source domain towards the target domain. We use the same splits as provided in the original paper [8]. The novel *HMDB-ARID* dataset is as introduced in Section 4, and also consist of two settings: HMDB→ARID and ARID→HMDB. For all four settings, we report the top-1 accuracy on the target dataset.

Our experiments are implemented using PyTorch [64] library. To obtain video features, we instantiate two 3D-CNNs, I3D [35] and MFNet [65], as G_f for both source domain videos and target domain videos. Both I3D and MFNet are utilized thanks to its performance on current action recognition benchmarks (namely UCF101 [63], HMDB51 [24] and Kinetics [66]). MFNet is also utilized due to its lightweight structure, which enables it to achieve comparable results to that of I3D while requiring a fraction of the parameters and computation power needed.

The source and target feature extractors share parameters. Following the implementation in [65, 35], the input for both I3D and MFNet are frame sequences of 16 frames with each frame of size 224×224 . The correlation extraction module takes the high-level video feature from the output of *layer4* in I3D and the output of *conv4* layer in MFNet as inputs, which are feature maps of size 14×14 . The stochastic gradient descent algorithm [67] is used for optimization, with the weight decay set to 0.0001 and the momentum to 0.9 for both I3D and MFNet. During training, the batch size is set to 8 samples per GPU. Our initial learning rate is set to 0.005 and is divided by 10 after 20 and 35 epochs. λ_v is set to 0.5 while λ_r and λ_d are both set to 1.0. All experiments are conducted using two NVIDIA GP100 GPUs.

5.2. Overall Results

There are limited studies focusing on applying DA approaches to the action recognition task. Here we first compare previous methods that utilizes the *UCF-HMDB_{full}* benchmark. This includes TA³N [8], TCoN [9] and SAVA [11]. Due to the different encoders used in experiments, we report both (a) “Source only” results, where the network is trained with supervised source data only and validated on the target data, and is the lower bound performance for the adaptation process; and (b) “Target only” results, where the network is directly trained and validated with supervised target data and is the upper bound performance for the adaptation process. The comparison of performance should focus on the networks’ improvement with respect to the performance with the “Source only” setting. The comparison should also focus on the distance between the network’s performance and the performance with the “Target only” setting. For the performance of TA³N, we follow the works in [11] and obtain the results by running the publicly available code. Table 3 shows the comparison of performances between our proposed ACAN and the methods as mentioned on *UCF-HMDB_{full}*.

The performance results in Table 3 shows that our proposed ACAN achieves the best result under the HMDB→UCF setting and very competitive perfor-

Method	Encoder	UCF→HMDB	HMDB→UCF
Source Only	TRN-Res101	73.1%	73.9%
TA ³ N	TRN-Res101	75.3%	79.3%
TCoN	TRN-Res101	87.2%	89.1%
Target Only	TRN-Res101	90.8%	95.6%
Source Only	I3D	80.3%	88.8%
SAVA	I3D	82.2%	91.2%
ACAN(Ours)	I3D	85.4%	93.8%
Target Only	I3D	95.0%	96.8%
Source Only	MFNet	78.6%	88.4%
ACAN(Ours)	MFNet	85.8%	93.2%
Target Only	MFNet	96.0%	97.1%

Table 3: Results on the two settings for *UCF-HMDB_{full}*

mance under the UCF→HMDB setting when using either MFNet and I3D as encoders. More specifically, our ACAN with the MFNet encoder achieves 85.8% top-1 accuracy for UCF→HMDB setting, indicating the improvement brought by ACAN towards the lower bound of the UCF→HMDB setting is 7.2%. This is significantly higher than that brought by SAVA (1.9%) and TA³N (2.2%). The large improvement brought by ACAN enables our network to perform better on UCF→HMDB setting despite the lower bound of MFNet is lower than that of I3D [35]. Under this setting, our ACAN is also closer to the upper bound of the encoder, with a gap of 10.2%. Comparatively, the gap to the upper bound performance is 15.5% for TA³N and 12.8% for SAVA. Similarly, our ACAN with I3D encoder also performs better than both TA³N and SAVA. Comparatively, ACAN with I3D encoder outperforms SAVA by a remarkable 3.2% while sharing the I3D as the common video feature encoder with SAVA. This further demonstrates the superiority of ACAN with respect to current video DA methods.

The superiority of ACAN further strengthens under the HMDB→UCF setting. Under this settings when utilizing MFNet as the video feature encoder,

Method	Encoder	HMDB→ ARID	ARID→ HMDB
Source Only	TRN-Res101	17.8%	15.7%
TA ³ N	TRN-Res101	22.4%	19.8%
Target Only	TRN-Res101	52.8%	50.9%
Source Only	MFNet	48.3%	37.9%
DANN	MFNet	50.7%	40.6%
MK-MMD	MFNet	50.2%	40.1%
MCD	MFNet	47.6%	36.8%
CORAL	MFNet	51.3%	41.7%
ACAN(Ours)	MFNet	58.0%	46.4%
Target Only	MFNet	76.1%	67.6%

Table 4: Results on the two settings for *HMDB-ARID*.

our proposed ACAN gains a 4.8% improvement towards the lower bound performance, which is greater than that brought by SAVA (2.4%). When utilizing I3D as the video feature encoder as in SAVA, our proposed ACAN gains an exceptional 5.0% improvement towards the lower bound performance. The larger increase built upon the strong I3D encoder enables our ACAN to achieve the best result under this setting achieving 93.8% top-1 accuracy utilizing I3D encoder. The gap towards the upper bound performance is also the smallest for ACAN using the I3D encoder, with 3.0% compared to 16.3% for TA³N, 6.5% for TCoN, and 5.6% for SAVA.

We further compare performance of several methods on our novel *HMDB-ARID* dataset, with both HMDB→ARID and ARID→HMDB settings, as shown in Table 4. Note that both settings are more challenging, given that the gap between the lower bound performance (trained with supervised source data) and the upper bound performance (trained with supervised target data) is larger compared to the settings for *UCF-HMDB_{full}*. In addition to comparing with the TA³N with TRN-Res101 [43] encoder, we also compare with performances with other typical DA approaches, e.g. DANN [1], MK-MMD [59], MCD [68], and CORAL [60], all with MFNet as the encoder.

The performance results in Table 4 indicate that our proposed ACAN achieves the best results in either setting related to our novel *HMDB-ARID* dataset. Our ACAN achieves a top-1 accuracy of 58.0% for the HMDB→ARID setting and 46.4% for the ARID→HMDB setting. Our ACAN also brings the most significant improvement with respect to the lower bound performance, with 9.8% and 8.5% for the two settings respectively. Comparatively, TA³N which does not utilize correlation alignment only brings 4.6% and 4.1% increase with respect to the lower bound performance. This shows that previous methods that fail to align correlations would not be able to handle the larger domain shift caused by a more significant difference in video statistics. Note that the gap to the upper bound performance obtained by training with supervised target data is still relatively large, suggesting further improvements could be made on this novel *HMDB-ARID* dataset.

5.3. Ablation Studies

We justify our proposed design of ACAN through thorough ablation studies. Specifically, we first examine the performance of our ACAN in four scenarios and justify the need for introducing correlation features in the extraction process, the use of two separate domain losses, and the introduction of PCD. We also introduce an alternative form of the joint correlation information distribution difference minimization to compare and justify our current design of PCD. All ablation studies are conducted under the UCF→HMDB and HMDB→ARID settings, with the batch size and other training parameters as mentioned in Section 5.1. The MFNet [65] is instantiated as the encoder for all ablation studies.

The necessity of correlation feature alignment. We first justify the need for correlation features for alignment, which is achieved by (a) comparing the “Source only” results with and without the introduction of correlation features, and (b) comparing the use of adversarial DA approaches with and without correlation features. Results in Table 5 justifies the use of correlation features, where the use of correlation features consistently improves the performance of

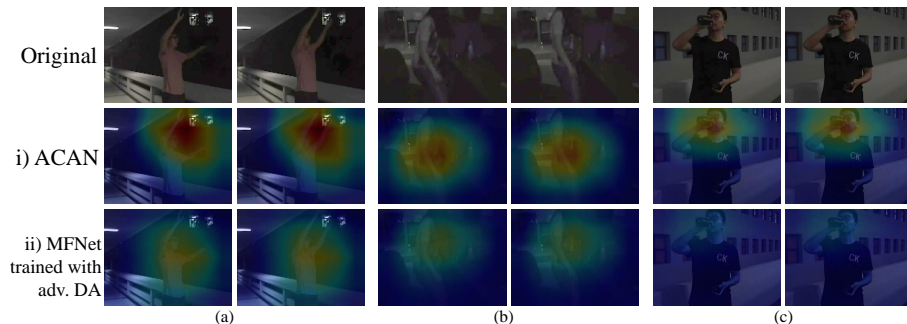


Figure 5: Class activation maps (CAMs) on ARID, utilizing i) ACAN and ii) MFNet trained with adversarial DA approach. The CAMs are obtained from three actions: (a) “Wave”; (b) “Stand”; and (c) “Drink”. We also show the original frames at the top row from which the CAMs are computed. The original frames are tuned brighter for visualization.

Method	UCF→HMDB	HMDB→ARID
Source only w/o. correlation	76.1%	48.1%
Source only w. correlation	78.6%	48.3%
Adv. DA w/o. correlation	80.2%	50.7%
Adv. DA w. correlation	84.2%	52.6%

Table 5: Ablation experiments on including correlation features, on UCF→HMDB and HMDB→ARID settings.

the network under both “Source only” training and when DANN method is used for DA. It could also be observed that the use of correlation features brings more improvement when the DANN method is applied. This is consistent with our argument of improving video feature alignment by using correlation alignment.

The effectiveness of domain loss \mathcal{L}_d . We then justify our design of the domain loss \mathcal{L}_d , which is the weighted sum of \mathcal{L}_{vd} and \mathcal{L}_{cd} . We compare with the variants of ACAN where either \mathcal{L}_{vd} or \mathcal{L}_{cd} alone is used for domain loss, denoted as ACAN $-\mathcal{L}_{cd}$ and ACAN $-\mathcal{L}_{vd}$. We also tested on the case where the domain loss is not applied (hence aligning correlation features by minimizing PCD alone), such a case is denoted as MFNet+PCD. As indicated in Table 6,

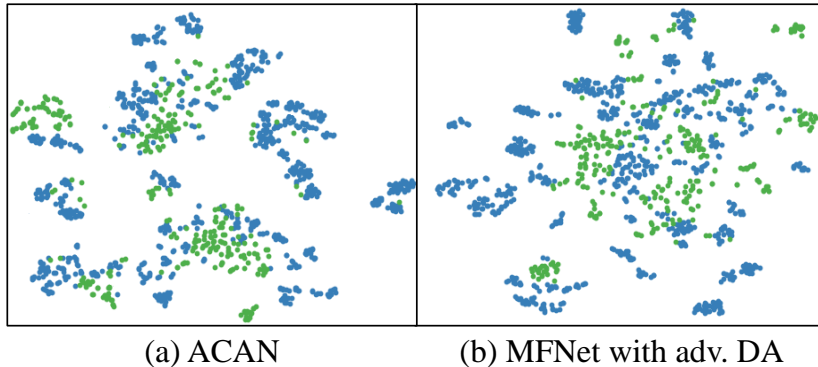


Figure 6: Comparison of t-SNE visualization of video features of both source and target domains under HMDB→ARID. The video features are obtained from (a) ACAN and (b) MFNet trained with the adversarial DA approach. The green dots represent the data from the source domain while the blue dots represent the data from the target domain.

Method	UCF→HMDB	HMDB→ARID
ACAN	85.8%	58.0%
ACAN - \mathcal{L}_{cd}	84.9%	56.9%
ACAN - \mathcal{L}_{vd}	84.5%	56.7%
MFNet + PCD	83.8%	56.1%

Table 6: Ablation experiments on the domain loss \mathcal{L}_d on UCF→HMDB and HMDB→ARID settings.

both losses contribute to the effective alignment of video features. The removal of either loss brings a decrease in network performance for both dataset settings. Further decrease is observed when no domain loss is applied. Meanwhile, the domain discriminators corresponding to either domain loss bring only a negligible growth in computation cost. Hence it is worthwhile to include two separate domain discriminators, with two domain losses for the overall domain loss \mathcal{L}_d .

The effectiveness of PCD. PCD is introduced for improving the effectiveness of correlation alignment by matching the joint correlation information distribution of video domains. We examine the effect of PCD through compar-

Method	UCF→HMDB	HMDB→ARID
ACAN	85.8%	58.0%
ACAN-Base	84.2%	52.6%
ACAN (l2-norm)	85.0%	54.2%

Table 7: Ablation on PCD and alternative way of minimizing joint correlation information distribution difference, on UCF→HMDB and HMDB→ARID settings.

ison with the ACAN variant without PCD, which is ACAN-Base as shown in Figure 2. The results in Table 7 demonstrates the effectiveness of PCD, whose absence caused a noticeable 1.6% decrease for UCF→HMDB setting, and a significant 5.4% decrease for HMDB→ARID setting. Though the introduced PCD improves the effectiveness of correlation alignment greatly, minimizing PCD involves kernel estimation which brings an increase in computation cost. Inspired by the hypothesis presented in [69], minimizing the joint distribution difference, and hence the distance between distributions p_{M_s} and p_{M_t} could also be achieved through matching the norm of p_{M_s} and p_{M_t} towards a shared restrictive scalar R . The computation of distribution distance with this method is simpler given that no kernel estimation is required. In this case, the equation for the overall loss Equation 13 is reformulated as:

$$\begin{aligned}
\mathcal{L} = & \mathcal{L}_y - (\lambda_v \mathcal{L}_{vd} + \lambda_r \mathcal{L}_{cd}) + \\
& \lambda_{dist} (L_{dist}(\frac{1}{N_s} \sum_{i=1}^{N_s} n(\mathbf{M}_s^i), R) + \\
& L_{dist}(\frac{1}{N_t} \sum_{j=1}^{N_t} n(\mathbf{M}_t^j), R)).
\end{aligned} \tag{14}$$

Here L_{dist} is the distance loss between the norm of PCMs and the restrictive scalar R , and is implemented as L_2 -distance, while $n(\cdot)$ denotes the norm function. R is set to 25 during the experiments. We denote the variant of ACAN with loss function in Equation 14 as ACAN (l2-norm) and compare with the original ACAN. The results shown in Table 7 shows that the variant formulated by Equation 14 could still bring noticeable improvement than that when the

distributions of p_{M_s} and p_{M_t} are not aligned. However, compared to PCD, the improvement is relatively minor. This further justifies the effectiveness of PCD.

5.4. Qualitative Analysis

To better understand the effect of ACAN, we perform qualitative analysis on trained networks. We first show the class activation maps (CAM) [70] of the target ARID videos with ACAN and with MFNet (encoder) trained with adversarial DA approach in Figure 5. The dark videos in ARID make it difficult for accurate video features to be extracted. Therefore if correlation alignment is not utilized, the network may fail to focus on the actual action in the target domain. It may rather briefly focus on the whole actor (Figure 5(ii-a)), or on unrelated background (Figure 5(ii-b)). With the involvement of correlation features and its alignment, ACAN is able to focus on the waving hand for the “Wave” action, or the person standing for the “Stand” action, thus showing much stronger performance on the HMDB→ARID setting. Further, we visualize the distribution of the source and target domains under the HMDB→ARID setting with t-SNE, as shown in Figure 6. It could be observed from Figure 6 that our proposed ACAN can group both the data from the source domain (green dots) and data from the target domain (blue dots) into denser clusters. Our ACAN could also match the target domain data with source domain data more accurately.

6. Conclusion and Future Work

In this work, we propose a novel domain adaptation method for action recognition across different domains. The new ACAN aligns correlation features in an adversarial manner while minimizing joint correlation information distribution differences by minimizing PCD. We further introduce a novel video DA dataset, *HMDB-ARID*, with a larger domain shift, and is the first video DA dataset that includes videos shot in adverse conditions. Our method obtains state-of-the-art result on both the *UCF-HMDB_{full}* and *HMDB-ARID* datasets. We further

justify our design through an ablation study and validate the effectiveness of ACAN with qualitative results.

Although state-of-the-art performances have been achieved by the proposed ACAN, we observe that the gap to the upper bound performance obtained by training with supervised target data is still relatively large as depicted in Table 4, suggesting further improvements could be made on the novel *HMDB-ARID* dataset. Additionally, cross-domain video datasets that involves a variety of large domain shift scenarios, such as blurry or hazy videos may be explored. Video DA approaches that cope with these different large domain shift scenarios would also be investigated.

References

- [1] Y. Ganin, V. Lempitsky, Unsupervised domain adaptation by backpropagation, in: International conference on machine learning, PMLR, 2015, pp. 1180–1189.
- [2] E. Tzeng, J. Hoffman, T. Darrell, K. Saenko, Simultaneous deep transfer across domains and tasks, in: Proceedings of the IEEE International Conference on Computer Vision, 2015, pp. 4068–4076.
- [3] X. Ma, T. Zhang, C. Xu, Deep multi-modality adversarial networks for unsupervised domain adaptation, *IEEE Transactions on Multimedia* 21 (9) (2019) 2419–2431.
- [4] Y. Chen, W. Li, C. Sakaridis, D. Dai, L. Van Gool, Domain adaptive faster r-cnn for object detection in the wild, in: Proceedings of the IEEE conference on computer vision and pattern recognition, 2018, pp. 3339–3348.
- [5] Q. Cai, Y. Pan, C.-W. Ngo, X. Tian, L. Duan, T. Yao, Exploring object relation in mean teacher for cross-domain detection, in: Proceedings of the IEEE Conference on Computer Vision and Pattern Recognition, 2019, pp. 11457–11466.
- [6] S. Song, Z. Miao, H. Yu, J. Fang, K. Zheng, C. Ma, S. Wang, Deep domain adaptation based multi-spectral salient object detection, *IEEE Transactions on Multimedia*.
- [7] F. Yang, K. Yan, S. Lu, H. Jia, D. Xie, Z. Yu, X. Guo, F. Huang, W. Gao, Part-aware progressive unsupervised domain adaptation for person re-identification, *IEEE Transactions on Multimedia*.
- [8] M.-H. Chen, Z. Kira, G. AlRegib, J. Yoo, R. Chen, J. Zheng, Temporal attentive alignment for large-scale video domain adaptation, in: Proceedings of the IEEE International Conference on Computer Vision, 2019, pp. 6321–6330.

- [9] B. Pan, Z. Cao, E. Adeli, J. C. Niebles, Adversarial cross-domain action recognition with co-attention., in: AAAI, 2020, pp. 11815–11822.
- [10] D. Xu, J. Xiao, Z. Zhao, J. Shao, D. Xie, Y. Zhuang, Self-supervised spatiotemporal learning via video clip order prediction, in: Proceedings of the IEEE Conference on Computer Vision and Pattern Recognition, 2019, pp. 10334–10343.
- [11] J. Choi, G. Sharma, S. Schuler, J.-B. Huang, Shuffle and attend: Video domain adaptation, in: European Conference on Computer Vision, Springer, 2020, pp. 678–695.
- [12] X. Wang, R. Girshick, A. Gupta, K. He, Non-local neural networks, in: Proceedings of the IEEE conference on computer vision and pattern recognition, 2018, pp. 7794–7803.
- [13] A. Buades, B. Coll, J.-M. Morel, A non-local algorithm for image denoising, in: 2005 IEEE Computer Society Conference on Computer Vision and Pattern Recognition (CVPR’05), Vol. 2, IEEE, 2005, pp. 60–65.
- [14] H. Li, C. Y. Suen, A novel non-local means image denoising method based on grey theory, *Pattern Recognition* 49 (2016) 237–248.
- [15] A. Vaswani, N. Shazeer, N. Parmar, J. Uszkoreit, L. Jones, A. N. Gomez, L. Kaiser, I. Polosukhin, Attention is all you need, in: Advances in neural information processing systems, 2017, pp. 5998–6008.
- [16] H. Chen, D. Jiang, H. Sahli, Transformer encoder with multi-modal multi-head attention for continuous affect recognition, *IEEE Transactions on Multimedia*.
- [17] Y. Zhang, Y. Gong, H. Zhu, X. Bai, W. Tang, Multi-head enhanced self-attention network for novelty detection, *Pattern Recognition* 107 (2020) 107486.

- [18] Y. Chen, Y. Kalantidis, J. Li, S. Yan, J. Feng, A²-nets: Double attention networks, in: *Advances in neural information processing systems*, 2018, pp. 352–361.
- [19] L. Wang, W. Li, W. Li, L. Van Gool, Appearance-and-relation networks for video classification, in: *Proceedings of the IEEE conference on computer vision and pattern recognition*, 2018, pp. 1430–1439.
- [20] K. Yue, M. Sun, Y. Yuan, F. Zhou, E. Ding, F. Xu, Compact generalized non-local network, in: *Advances in Neural Information Processing Systems*, 2018, pp. 6510–6519.
- [21] N. Lu, W. Yu, X. Qi, Y. Chen, P. Gong, R. Xiao, Master: Multi-aspect non-local network for scene text recognition, *Pattern Recognition* (2021) 107980.
- [22] J. A. Rice, *Mathematical statistics and data analysis*, Cengage Learning, 2006.
- [23] R. A. Horn, C. R. Johnson, *Matrix analysis*, Cambridge university press, 2012.
- [24] H. Kuehne, H. Jhuang, E. Garrote, T. Poggio, T. Serre, Hmdb: a large video database for human motion recognition, in: *2011 International Conference on Computer Vision*, IEEE, 2011, pp. 2556–2563.
- [25] Y. Xu, J. Yang, H. Cao, K. Mao, J. Yin, S. See, Arid: A new dataset for recognizing action in the dark, *arXiv preprint arXiv:2006.03876*.
- [26] K. Simonyan, A. Zisserman, Two-stream convolutional networks for action recognition in videos, in: *Advances in neural information processing systems*, 2014, pp. 568–576.
- [27] C. Feichtenhofer, A. Pinz, R. P. Wildes, Spatiotemporal multiplier networks for video action recognition, in: *Proceedings of the IEEE conference on computer vision and pattern recognition*, 2017, pp. 4768–4777.

- [28] A. Tran, L.-F. Cheong, Two-stream flow-guided convolutional attention networks for action recognition, in: Proceedings of the IEEE International Conference on Computer Vision Workshops, 2017, pp. 3110–3119.
- [29] X. Wang, L. Gao, P. Wang, X. Sun, X. Liu, Two-stream 3-d convnet fusion for action recognition in videos with arbitrary size and length, IEEE Transactions on Multimedia 20 (3) (2017) 634–644.
- [30] Y. Zhu, Z. Lan, S. Newsam, A. Hauptmann, Hidden two-stream convolutional networks for action recognition, in: Asian Conference on Computer Vision, Springer, 2018, pp. 363–378.
- [31] L. Wang, Y. Xiong, Z. Wang, Y. Qiao, D. Lin, X. Tang, L. Van Gool, Temporal segment networks for action recognition in videos, IEEE transactions on pattern analysis and machine intelligence 41 (11) (2018) 2740–2755.
- [32] Z. Tu, W. Xie, Q. Qin, R. Poppe, R. C. Veltkamp, B. Li, J. Yuan, Multi-stream cnn: Learning representations based on human-related regions for action recognition, Pattern Recognition 79 (2018) 32–43.
- [33] D. Tran, L. Bourdev, R. Fergus, L. Torresani, M. Paluri, Learning spatiotemporal features with 3d convolutional networks, in: Proceedings of the IEEE international conference on computer vision, 2015, pp. 4489–4497.
- [34] D. Tran, J. Ray, Z. Shou, S.-F. Chang, M. Paluri, Convnet architecture search for spatiotemporal feature learning, arXiv preprint arXiv:1708.05038.
- [35] J. Carreira, A. Zisserman, Quo vadis, action recognition? a new model and the kinetics dataset, in: proceedings of the IEEE Conference on Computer Vision and Pattern Recognition, 2017, pp. 6299–6308.
- [36] K. Liu, W. Liu, C. Gan, M. Tan, H. Ma, T-c3d: Temporal convolutional 3d network for real-time action recognition, in: Thirty-second AAAI conference on artificial intelligence, 2018, pp. 7138–7145.

- [37] K. Hara, H. Kataoka, Y. Satoh, Can spatiotemporal 3d cnns retrace the history of 2d cnns and imagenet?, in: Proceedings of the IEEE conference on Computer Vision and Pattern Recognition, 2018, pp. 6546–6555.
- [38] H. Yang, C. Yuan, B. Li, Y. Du, J. Xing, W. Hu, S. J. Maybank, Asymmetric 3d convolutional neural networks for action recognition, Pattern recognition 85 (2019) 1–12.
- [39] J. Li, X. Liu, W. Zhang, M. Zhang, J. Song, N. Sebe, Spatio-temporal attention networks for action recognition and detection, IEEE Transactions on Multimedia 22 (11) (2020) 2990–3001.
- [40] D. Tran, H. Wang, L. Torresani, J. Ray, Y. LeCun, M. Paluri, A closer look at spatiotemporal convolutions for action recognition, in: Proceedings of the IEEE conference on Computer Vision and Pattern Recognition, 2018, pp. 6450–6459.
- [41] S. Xie, C. Sun, J. Huang, Z. Tu, K. Murphy, Rethinking spatiotemporal feature learning: Speed-accuracy trade-offs in video classification, in: Proceedings of the European Conference on Computer Vision (ECCV), 2018, pp. 305–321.
- [42] C.-Y. Ma, A. Kadav, I. Melvin, Z. Kira, G. AlRegib, H. Peter Graf, Attend and interact: Higher-order object interactions for video understanding, in: Proceedings of the IEEE Conference on Computer Vision and Pattern Recognition, 2018, pp. 6790–6800.
- [43] B. Zhou, A. Andonian, A. Oliva, A. Torralba, Temporal relational reasoning in videos, in: Proceedings of the European Conference on Computer Vision (ECCV), 2018, pp. 803–818.
- [44] I. Goodfellow, J. Pouget-Abadie, M. Mirza, B. Xu, D. Warde-Farley, S. Ozair, A. Courville, Y. Bengio, Generative adversarial nets, in: Advances in neural information processing systems, 2014, pp. 2672–2680.

- [45] E. Tzeng, J. Hoffman, K. Saenko, T. Darrell, Adversarial discriminative domain adaptation, in: Proceedings of the IEEE conference on computer vision and pattern recognition, 2017, pp. 7167–7176.
- [46] J. Hoffman, E. Tzeng, T. Park, J.-Y. Zhu, P. Isola, K. Saenko, A. Efros, T. Darrell, Cycada: Cycle-consistent adversarial domain adaptation, in: International conference on machine learning, PMLR, 2018, pp. 1989–1998.
- [47] H. Zou, Y. Zhou, J. Yang, H. Liu, H. P. Das, C. J. Spanos, Consensus adversarial domain adaptation, in: Proceedings of the AAAI Conference on Artificial Intelligence, Vol. 33, 2019, pp. 5997–6004.
- [48] J. Zhang, W. Li, P. Ogunbona, Joint geometrical and statistical alignment for visual domain adaptation, in: Proceedings of the IEEE Conference on Computer Vision and Pattern Recognition, 2017, pp. 1859–1867.
- [49] X. Zhu, J. Pang, C. Yang, J. Shi, D. Lin, Adapting object detectors via selective cross-domain alignment, in: Proceedings of the IEEE Conference on Computer Vision and Pattern Recognition, 2019, pp. 687–696.
- [50] Y. Zou, Z. Yu, B. Vijaya Kumar, J. Wang, Unsupervised domain adaptation for semantic segmentation via class-balanced self-training, in: Proceedings of the European conference on computer vision (ECCV), 2018, pp. 289–305.
- [51] T.-H. Vu, H. Jain, M. Bucher, M. Cord, P. Pérez, Dada: Depth-aware domain adaptation in semantic segmentation, in: Proceedings of the IEEE International Conference on Computer Vision, 2019, pp. 7364–7373.
- [52] Y.-C. Chen, Y.-Y. Lin, M.-H. Yang, J.-B. Huang, Crdoco: Pixel-level domain transfer with cross-domain consistency, in: Proceedings of the IEEE Conference on Computer Vision and Pattern Recognition, 2019, pp. 1791–1800.
- [53] D. Guan, J. Huang, S. Lu, A. Xiao, Scale variance minimization for unsupervised domain adaptation in image segmentation, Pattern Recognition 112 (2021) 107764.

- [54] R. Panda, A. Bhuiyan, V. Murino, A. K. Roy-Chowdhury, Adaptation of person re-identification models for on-boarding new camera (s), *Pattern Recognition* 96 (2019) 106991.
- [55] A. Jamal, V. P. Namboodiri, D. Deodhare, K. Venkatesh, Deep domain adaptation in action space., in: *BMVC*, 2018, p. 264.
- [56] M.-H. Chen, B. Li, Y. Bao, G. AlRegib, Z. Kira, Action segmentation with joint self-supervised temporal domain adaptation, in: *Proceedings of the IEEE/CVF Conference on Computer Vision and Pattern Recognition*, 2020, pp. 9454–9463.
- [57] L. Fu, T. H. Nguyen, B. Min, R. Grishman, Domain adaptation for relation extraction with domain adversarial neural network, in: *Proceedings of the Eighth International Joint Conference on Natural Language Processing (Volume 2: Short Papers)*, 2017, pp. 425–429.
- [58] Y. Li, N. Wang, J. Liu, X. Hou, Demystifying neural style transfer, *arXiv preprint arXiv:1701.01036*.
- [59] M. Long, Y. Cao, J. Wang, M. Jordan, Learning transferable features with deep adaptation networks, in: *International conference on machine learning*, PMLR, 2015, pp. 97–105.
- [60] B. Sun, K. Saenko, Deep coral: Correlation alignment for deep domain adaptation, in: *European conference on computer vision*, Springer, 2016, pp. 443–450.
- [61] W. Sultani, I. Saleemi, Human action recognition across datasets by foreground-weighted histogram decomposition, in: *Proceedings of the IEEE Conference on Computer Vision and Pattern Recognition*, 2014, pp. 764–771.
- [62] T. Xu, F. Zhu, E. K. Wong, Y. Fang, Dual many-to-one-encoder-based transfer learning for cross-dataset human action recognition, *Image and Vision Computing* 55 (2016) 127–137.

- [63] K. Soomro, A. R. Zamir, M. Shah, Ucf101: A dataset of 101 human actions classes from videos in the wild, arXiv preprint arXiv:1212.0402.
- [64] A. Paszke, S. Gross, F. Massa, A. Lerer, J. Bradbury, G. Chanan, T. Killeen, Z. Lin, N. Gimelshein, L. Antiga, et al., Pytorch: An imperative style, high-performance deep learning library, in: Advances in neural information processing systems, 2019, pp. 8026–8037.
- [65] Y. Chen, Y. Kalantidis, J. Li, S. Yan, J. Feng, Multi-fiber networks for video recognition, in: Proceedings of the european conference on computer vision (ECCV), 2018, pp. 352–367.
- [66] W. Kay, J. Carreira, K. Simonyan, B. Zhang, C. Hillier, S. Vijayanarasimhan, F. Viola, T. Green, T. Back, P. Natsev, et al., The kinetics human action video dataset, arXiv preprint arXiv:1705.06950.
- [67] L. Bottou, Large-scale machine learning with stochastic gradient descent, in: Proceedings of COMPSTAT’2010, Springer, 2010, pp. 177–186.
- [68] K. Saito, K. Watanabe, Y. Ushiku, T. Harada, Maximum classifier discrepancy for unsupervised domain adaptation, in: Proceedings of the IEEE Conference on Computer Vision and Pattern Recognition, 2018, pp. 3723–3732.
- [69] R. Xu, G. Li, J. Yang, L. Lin, Larger norm more transferable: An adaptive feature norm approach for unsupervised domain adaptation, in: Proceedings of the IEEE International Conference on Computer Vision, 2019, pp. 1426–1435.
- [70] B. Zhou, A. Khosla, A. Lapedriza, A. Oliva, A. Torralba, Learning deep features for discriminative localization, in: Proceedings of the IEEE conference on computer vision and pattern recognition, 2016, pp. 2921–2929.